Renewable Energy 117 (2018) 202–216

Contents lists available at ScienceDirect

Renewable Energy

journal homepage: www.elsevier.com/locate/renene

Experimental validation of an analytical model for performance estimation of natural convection solar air heating collectors

Alejandro L. Hernández*, José E. Quiñonez

National University of Salta (UNSa), Non Conventional Energy Research Institute (INENCO), National Scientific and Technical Research Council (CONICET), Av. Bolivia N° 5.150, A4408FVY, Salta, Argentina

ARTICLE INFO

Article history:
Received 12 June 2017
Received in revised form
27 August 2017
Accepted 28 September 2017
Available online 30 September 2017

Keywords:
Solar air collector
Mathematical modelling
Experimental validation

ABSTRACT

In this paper, the experimental validation of an analytical model that describes the thermal behaviour of double parallel flow air heating collectors working by natural convection is presented. This model was validated with data measured on a collector of these characteristics at the National University of Salta, in the northwest of Argentina. Comparisons between measured and simulated values show an excellent agreement for both the air output temperature and the useful energy produced by the collector, with *RMSE* values smaller than 6%. The instantaneous thermal efficiency curve of the collector was determined experimentally in winter of 2015. Daily values of efficiency ranged between 0.48 and 0.5 during sunny days, and between 0.41 and 0.46 during semi-cloudy days. A novel correlation between the velocity of the air movement by natural convection and the temperature difference between the building and the collector's interior was obtained by means of linear regression with a correlation coefficient $R^2 = 0.94$. A new correlation $Nu = f(Ra)$ to estimate the average convective coefficients by natural convection was obtained, based on an effective convective heat transfer coefficient calculated with the temperature values measured inside the collector and the absorbed solar irradiance.

1. Introduction

Since the middle of last century, the solar air heating has aroused great interest in the community of solar researchers because it is a relatively simple, inexpensive and low maintenance application. Along these years, several prototypes of solar air collectors were designed, mathematically modelled and experimentally tested. These air heaters are mainly used to dry agricultural products [1–3] and to heat buildings [4–7]. There are many configurations of solar air heater collectors, differentiated by the way the air circulates inside (natural or forced convection in simple pass, double parallel flow, double pass counter flow, etc.) and the type of solar absorber element (flat plate, V-corrugated plate, cylindrical tubes, plates with fins, porous matrix, etc.) [8–13].

Each type of collector has a particular efficiency of conversion of solar energy into heat which depends on its geometry, materials with which it is built, the site location, the time of the year and the air mass flow circulating inside. The most important disadvantage of air heating collectors against water heating collectors is the poor heat transfer existing between the absorber plates and circulating air due to the low convective heat transfer coefficient that characterizes to gaseous fluids. Therefore, to achieve high rates of thermal energy transfer it is convenient to use, as absorber element, extended surfaces with large areas exposed to the heat carrying fluid to improve the heat removal factor of the collector, F_R. The more efficient air heating collectors are those maximizing the contact between the circulating air and the absorber plate by means of forced turbulent flow in double pass including V-corrugated or sine-wave absorber plates, with fins, baffles, ribs or porous matrices [14–21]. With this type of collectors, thermal efficiencies up to 80%have been achieved. In Ref. [6], a two-story bioclimatic building constructed in Vaqueros town, near to Salta City, is described. The bioclimatic strategies selected to heat the building were: thermal insulation of the outer walls and roof, direct solar gain by windows in the bedrooms located to the north and a double pass counter flow solar air heater collector included in the roof to heat the dining room and the living room, both located to the south. The absorber plate of the solar collector is a 24 m^2 black painted V-corrugated galvanized iron sheet. The air flows forced by a fan at a mass flow of 0.41 kg/s. During a sunny day in winter, this solar

* Corresponding author. National University of Salta, 5.150 Bolivia Avenue, Salta Capital, A4408FVY, Salta, Argentina.
E-mail address: alejoher65@gmail.com (A.L. Hernández).

https://doi.org/10.1016/j.renene.2017.09.082
0960-1481/

Nomenclature

L	length of solar collector in the direction of flow in m
w	width of solar collector in m
b	flow channel height in m (distance between the transparent cover and the bottom of the collector)
D_h	hydraulic diameter of the flow channel in m
A_c	aperture area of the collector (L x w) in m^2
A_i	cross-sectional area of the inlet duct of collector in m^2
A_{c1}	area of the transparent cover
A_p	area of the absorber plate
A_b	area of the bottom plate
H	altitude above sea level of the location of solar collector in m
h_1	convection heat transfer coefficient under the transparent cover in W/(m^2 °C)
h_2 and h_3	convection heat transfer coefficients on each side of absorber plate in W/(m^2 °C)
h_4	convection heat transfer coefficients over the bottom surface in W/(m^2 °C)
h_{eff}	effective heat transfer coefficient
h_{r1}	radiation heat transfer coefficients between the absorber plate and the cover in W/(m^2 °C)
h_{r2}	radiation heat transfer coefficients between the absorber plate and the bottom surface in W/(m^2 °C)
U_t	top loss coefficient from the transparent cover to the ambient in W/(m^2 °C)
U_b	back loss coefficient from the bottom surface to the ambient in W/(m^2 °C)
U_L	overall heat loss coefficient of the collector in W/(m^2 °C)
$\dot{m}_1$ and $\dot{m}_2$	mass flows of air in each channel of double-parallel flow solar collector in kg/s
$\dot{m}$	total mass flow of air entering and leaving the collector in kg/s
F'	collector efficiency factor
F_R	collector heat removal factor
F_{12}	view factor of the cover and bottom with the absorber plate
R_b	geometric factor that transforms the direct irradiance on horizontal plane into direct irradiance on tilted plane
T_{f1}	local temperature of the air flowing between the absorber plate and the cover in °C
T_{f2}	local temperature of the air flowing between the absorber plate and the bottom surface in °C
T_{c1}	local temperature of the inner transparent cover in °C
T_p	local temperature of the absorber plate in °C
T_b	local temperature of the bottom surface of the collector in °C
T_i	input air temperature to the collector in °C
T_o	output air temperature from the collector in °C
T_a	outside environment temperature in °C
T_l	inner temperature of the building
G_b	direct solar irradiance on horizontal plane in W/m^2
G_{ds}	isotropic diffuse solar irradiance of sky on horizontal plane in W/m^2
G_h	global solar irradiance on horizontal plane in W/m^2
G_p	total solar irradiance on the tilted plane of collector in W/m^2
S	solar irradiance absorbed by the absorber plate in W/m^2
q_{u1}	useful energy gain of the air flowing between the absorber plate and the cover in W/m^2
q_{u2}	useful energy gain of the air flowing between the absorber plate and the bottom surface in W/m^2
Q_u	total useful energy gain in W
k	thermal conductivity of air in W/(m K)
ρ	density of air in kg/m^3
c_p	specific heat at constant pressure of air in J/(kg K)
ν	kinematic viscosity of air in m^2/s
α	thermal diffusivity of air in m^2/s
β	volumetric thermal expansion coefficient of air in K^{-1}
$P(H)$	atmospheric pressure at height H above sea level, in Pa
v_i	air velocity in the inlet duct of the collector in m/s
g	gravity acceleration in m/s^2
η_c	instantaneous efficiency of the solar collector
α_p	solar absorptance of the absorber plate
β_c	slope of collector from the horizontal plane in degrees (90° in this case)
ε_{c1}	infrared emittance of the internal sheet of transparent cover
ε_p	infrared emittance of the absorber plate
ε_b	infrared emittance of the bottom plate
ρ_g	ground reflectance (albedo)
τ_b	transmittance of the transparent cover to direct solar irradiance
τ_d	transmittance of the cover to the sky diffuse solar irradiance
τ_g	transmittance of the cover to the ground diffuse solar irradiance

collector generated between 350 y 410 MJ of thermal energy with a daily efficiency of 73%.

While there are many works in the literature on air heating collectors operating with forced flow by blowers or fans, few researchers paid attention to collectors functioning by natural convection, probably because their thermal performances are lower than those of forced flow. But this should be not a barrier to its application because the collectors operated by natural convection have the advantage of not using electrical power to impulse the air, minimizing thus the operation and maintenance costs. Also, they do not require a manual or automatic control system for turning *on* and *off*, freeing the user to address this task. Numerical studies have been conducted to investigate the natural convection inside the channel between the flat-plate cover and the sine-wave absorber in a cross-corrugated solar air heater [22,23]. Hatami and Bahadorinejad [24] experimentally determined the natural convection heat transfer coefficient in a vertical flat-plate solar air heater with double transparent cover. They studied six flow configurations and concluded that the highest thermal efficiency is obtained when air flows through three parallel channels: between the absorber plate and the bottom of the collector, between the absorber plate and the inner transparent cover and between the inner and outer covers. Al-Kayiem and Yassen [25] experimentally studied the natural convection heat transfer in a flat-plate solar air heater tilted a θ angle. They presented the results by means of *Nu* vs Ra graphs and *Nu* vs time graphs for three inclination angles: 30°, 50° and 70°. They concluded that the optimum inclination angle of the collector is approximately 50° to obtain a high Nusselt number and the

highest collector efficiency. Hernández et al. [26] designed and experimentally tested a vertical solar air heater collector with perforated absorber plate which operates by natural convection and obtained values of daily thermal efficiency of between 57 and 60% for winter period. These values are significantly high and indicate that it is feasible to use this technology for passive heating of residential and industrial buildings.

The computational modelling is critical in order to simulate the operation of the solar collector under different weather conditions and at different latitudes. The mathematical expressions obtained with the analytical models allow to develop useful computational tools to design solar collectors, as well as, to evaluate its performances under different operating conditions without the need to build any real prototype [27–30]. Once developed the mathematical models, it is necessary to experimentally validate them in order to delimit the accuracy of their predictions and check the validity of the simplifying assumptions made during their formulation [31–36].

The authors of this paper have developed analytical models to assess the thermal performance of air heating collectors of double parallel flow and double pass counter flow [37]. The model corresponding to the double pass solar collectors was experimentally validated in a previous work [38], operating with forced flow under winter weather conditions of Salta City, located in the northwest of Argentina. The model validation was performed by comparing measured and simulated data of the output air temperature and useful energy. The results show an excellent agreement between the measured data and the simulated values with the model. The *RMSE* error was lower than 2.93 °C for the output air temperature and lower than 36.5 W for the useful energy.

In this paper, the experimental validation of the analytical model developed in Ref. [37] for the double parallel flow solar air collector, working by natural convection, is presented. Temperature values of the air output and the useful energy gain estimated through the model were compared with data measured in July 2015 in a solar collector of this type designed and built by the authors of this work at the National University of Salta. This prototype was vertically installed on the north facade (toward the Ecuador) of an experimental building so that its thermal energetic assessment was performed under real operating conditions (closed circuit collector-building), allowing to analyze the thermal dynamics of the whole system. Most experimental studies of solar air collectors are performed in open circuit (taking outside air, heating it and expelling it to the outside environment again) so that the results obtained in this work are an important contribution to the study of this type of solar technology.

The model is valid for both flow by natural convection and by forced flow. In the first case, the air velocity depends on the temperature of the absorber plate and, therefore, varies along the hours of sunshine. It was not found in the literature a correlation that allows the evaluation of this velocity to calculate the mass flow of the air passing through the collector. Therefore, a new empirical correlation that estimates the thermo-siphonic air velocity at the collector inlet, depending on the temperature difference between the interior of the collector and the interior of the building to be heated, was determined. Finally, a new methodology to estimate the internal convective coefficients on the absorber plate, the transparent cover and the bottom surface of the collector was developed and a new empirical correlation between dimensionless numbers *Nu* and *Ra*, valid in the range $2.5 \times 10^5 < Ra < 1.3 \times 10^6$, was obtained from the data measured during the monitoring campaign.

2. Synthesis of the analytical model of double parallel flow solar air collectors

The mathematical model evaluated in this paper has been developed by the authors and detailed in a previous paper [37]. It starts from the energy balance in steady state for the air flowing inside the solar collector to determine the overall heat loss coefficient, U_L, and its efficiency factor F'. In Fig. 1, the heat transfer coefficients included in the equations are shown. The dashed line represents the transparent cover.

If the collector cover consists of two or more sheets of transparent material, the coefficient U_t quantifies the heat loss from the inner sheet, which is at temperature T_{c1}, to the outside ambient temperature T_a.

At some location along the flow direction, the energy balances in steady state for the transparent cover, the air passing through channel 1, the absorber plate, the air passing through channel 2 and the bottom surface of the collector respectively are:

$$U_t(T_a - T_{c1}) + h_1\left(T_{f1} - T_{c1}\right) + h_{r1}(T_p - T_{c1}) = 0 \tag{1}$$

$$h_1\left(T_{c1} - T_{f1}\right) + h_2\left(T_p - T_{f1}\right) = q_{u1} \tag{2}$$

$$S + h_2\left(T_{f1} - T_p\right) + h_{r1}(T_{c1} - T_p) + h_3\left(T_{f2} - T_p\right) + h_{r2}(T_b - T_p) = 0 \tag{3}$$

$$h_3\left(T_p - T_{f2}\right) + h_4\left(T_b - T_{f2}\right) = q_{u2} \tag{4}$$

$$U_b(T_a - T_b) + h_4\left(T_{f2} - T_b\right) + h_{r2}(T_p - T_b) = 0 \tag{5}$$

Solving this equation system, the total useful energy locally gained by the fluid passing through the collector is:

$$q_u = q_{u1} + q_{u2} = F'\left[S - U_{01}\left(T_{f1} - T_a\right) - U_{02}\left(T_{f2} - T_a\right)\right] \tag{6}$$

where

$$F' = \frac{(h_2 + h_3)\Sigma_1\Sigma_2 + h_1h_{r1}\Sigma_2 + h_4h_{r2}\Sigma_1}{\Sigma_3} \quad \text{(efficiency factor)} \tag{7}$$

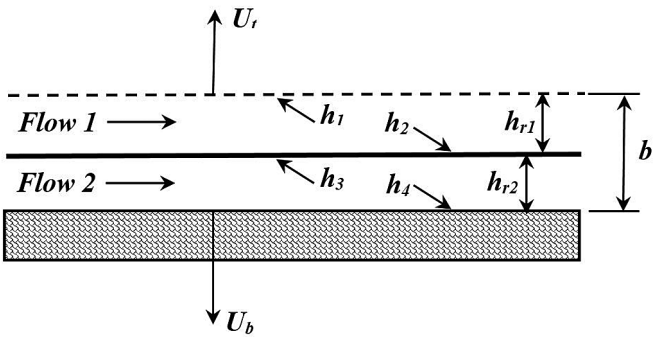

Fig. 1. Details of the heat transfer coefficients inside the solar collector.

$$U_{01} = \frac{h_1 U_t \Sigma_3 + (h_2 \Sigma_1 + h_1 h_{r1})(h_{r1} U_t \Sigma_2 + h_{r2} U_b \Sigma_1)}{[(h_2 + h_3)\Sigma_1 \Sigma_2 + h_1 h_{r1} \Sigma_2 + h_4 h_{r2} \Sigma_1]\Sigma_1} \quad (8)$$

$$U_{02} = \frac{h_4 U_b \Sigma_3 + (h_3 \Sigma_2 + h_4 h_{r2})(h_{r1} U_t \Sigma_2 + h_{r2} U_b \Sigma_1)}{[(h_2 + h_3)\Sigma_1 \Sigma_2 + h_1 h_{r1} \Sigma_2 + h_4 h_{r2} \Sigma_1]\Sigma_2} \quad (9)$$

being

$$\Sigma_1 = U_t + h_1 + h_{r1} \quad (10)$$

$$\Sigma_2 = U_b + h_4 + h_{r2} \quad (11)$$

$$\Sigma_3 = (h_2 + h_3)\Sigma_1 \Sigma_2 + h_{r1}(U_t + h_1)\Sigma_2 + h_{r2}(U_b + h_4)\Sigma_1 \quad (12)$$

Defining the overall heat loss coefficient of the collector, U_L, as

$$U_L = U_{01} + U_{02} \quad (13)$$

Eq. (6) can be written as

$$q_u = F'\left[S - U_L\left(\left\langle T_f \right\rangle - T_a\right)\right] \quad (14)$$

where

$$\left\langle T_f \right\rangle = \frac{U_{01} T_{f1} + U_{02} T_{f2}}{U_L} \quad (15)$$

is the average temperature of the fluid in some location inside the collector. Eq. (14) is an equivalent expression to the useful energy locally gained by a fluid passing through a collector of a single channel.

To estimate each convection heat transfer coefficients inside both channels of the collector (h_1 to h_4) it is necessary to calculate the mean values of T_{f1} and T_{f2} between the air inlet and outlet positions. To do that, the distribution of these temperatures along the collector in the direction of flow (y) must be found, resulting:

$$T_{f1}(y) = K_1 \exp(\alpha_1 y) + K_2 \exp(\alpha_2 y) + C \quad (16)$$

$$T_{f2}(y) = K_1 \exp(\alpha_1 y) - \frac{U_{01}}{U_{02}} K_2 \exp(\alpha_2 y) + D \quad (17)$$

where

$$\alpha_1 = -\frac{A_c F' U_L}{\dot{m} c_p L} \quad (18)$$

$$\alpha_2 = -\frac{A_c F' U_L}{\dot{m} c_p L}\left(1 + \frac{U_L U_{12}^1}{U_{02} U'_{01}}\right) \quad (19)$$

$$K_1 = T_i - T_a - \frac{S}{U_L}\left[\frac{U'_{01} U'_{02} + U_L\left(U_{12}^1 + U_{12}^2\right)}{U'_{01} U'_{02} + U_{12}^1 U'_{02} + U_{12}^2 U'_{01}}\right] \quad (20)$$

$$K_2 = \frac{S}{U_L}\left[\frac{U_{02}(U'_{01} - U'_{02})}{U'_{01} U'_{02} + U_{12}^1 U'_{02} + U_{12}^2 U'_{01}}\right] \quad (21)$$

$$C = T_a + \left(\frac{U'_{02} + U_{12}^1 + U_{12}^2}{U'_{01} U'_{02} + U_{12}^1 U'_{02} + U_{12}^2 U'_{01}}\right) S \quad (22)$$

$$D = T_a + \left(\frac{U'_{01} + U_{12}^1 + U_{12}^2}{U'_{01} U'_{02} + U_{12}^1 U'_{02} + U_{12}^2 U'_{01}}\right) S \quad (23)$$

$$U'_{01} = \frac{h_1 U_t \Sigma_3 + (h_2 \Sigma_1 + h_1 h_{r1})(h_{r1} U_t \Sigma_2 + h_{r2} U_b \Sigma_1)}{(h_2 \Sigma_1 \Sigma_2 + h_1 h_{r1} \Sigma_2)\Sigma_1} \quad (24)$$

$$U'_{02} = \frac{h_4 U_b \Sigma_3 + (h_3 \Sigma_2 + h_4 h_{r2})(h_{r1} U_t \Sigma_2 + h_{r2} U_b \Sigma_1)}{(h_3 \Sigma_1 \Sigma_2 + h_4 h_{r2} \Sigma_1)\Sigma_2} \quad (25)$$

$$U_{12}^1 = \frac{h_3 \Sigma_2 + h_4 h_{r2}}{\Sigma_2} \quad (26)$$

$$U_{12}^2 = \frac{h_2 \Sigma_1 + h_1 h_{r1}}{\Sigma_1} \quad (27)$$

The different heat transfer coefficients involved in the operation of the collector must be estimated at the mean temperature of the air passing through each channel. These average values are obtained by integrating the spatial distributions of these temperatures, Eq. (16) y (17), between the air inlet and outlet resulting:

$$\overline{T}_{f1} = C - \frac{K_1}{\alpha_1 L}[1 - \exp(\alpha_1 L)] - \frac{K_2}{\alpha_2 L}[1 - \exp(\alpha_2 L)] \quad (28)$$

and

$$\overline{T}_{f2} = D - \frac{K_1}{\alpha_1 L}[1 - \exp(\alpha_1 L)] + \frac{K_2 U_{01}}{\alpha_2 L U_{02}}[1 - \exp(\alpha_2 L)] \quad (29)$$

These mean temperatures are necessary to calculate the convective heat transfer coefficients h_1 to h_4, the coefficients U_{01}, U_{02}, U_L, F', U'_{01}, U'_{02}, U_{12}^1, $U_{12}^2$and temperatures T_{c1}, T_p and T_b. Nevertheless, to compute Eqs. (16) and (17) it is necessary to know the values of all these coefficients. Therefore, an iterative procedure must be performed by proposing initial values of $\overline{T}_{f1}$ y $\overline{T}_{f2}$ to calculate all coefficients and temperatures required to compute Eqs. (28) and (29). These new values of mean temperatures are compared with those originally proposed. If their differences are below a value considered appropriate (e.g. 0.1 °C) the iteration ends. Otherwise, the initial and recalculated mean temperatures are averaged and a new iteration begins.

The analytical model predicts that the air mass flows in each channel within the solar collector can be estimated as

$$\dot{m}_1 = \frac{U_{01}}{U_L} \cdot \dot{m} \quad (30)$$

and

$$\dot{m}_2 = \frac{U_{02}}{U_L} \cdot \dot{m} \quad (31)$$

According to their mathematical expressions $U_{01} > U_{02}$ because, generally, $U_t \gg U_b$. Therefore, the air mass flow in the channel formed by the transparent cover and the absorber plate, $\dot{m}_1$, is greater than the air mass flow in the other channel. These air mass flows are necessary to estimate the convective heat transfer coefficients h_1 to h_4.

The spatial distribution of the average air temperature inside the collector (as a weighted average of air temperatures in each channel) is

$$\left\langle T_f \right\rangle(y) = T_a + \frac{S}{U_L} + \left(T_i - T_a - \frac{S}{U_L}\right)\exp\left(-\frac{wF'U_L}{\dot{m}c_p} y\right) \quad (32)$$

This expression allows to estimate the air outlet temperature when it is evaluated at $y = L$. Thus, the temperature of the air leaving the collector, which results from the mixture of the two currents flowing inside it, is given by

$$T_o = T_a + \frac{S}{U_L} + \left(T_i - T_a - \frac{S}{U_L}\right)\exp\left(-\frac{A_c F' U_L}{\dot{m} c_p}\right) \tag{33}$$

This equation states that the air outlet temperature depends on T_i, T_a, S and $\dot{m}$ which, under steady state conditions, are considered constant within a finite time interval but variables from sunrise to sunset.

The total useful energy gain of solar collector may be expressed as [41]

$$Q_u = \dot{m} c_p (T_o - T_i) = A_c F_R [S - U_L (T_i - T_a)] \tag{34}$$

The heat removal factor, F_R, relates the actual useful energy gain of the collector to the useful gain if the whole collector were at the input air temperature. For a double parallel flow solar collector its expression is

$$F_R = \frac{\dot{m} c_p}{A_c U_L}\left[1 - \exp\left(-\frac{A_c F' U_L}{\dot{m} c_p}\right)\right] \tag{35}$$

with F' from Eq. (7) and U_L from Eq. (13). By defining this coefficient, the useful energy gain is expressed in terms of the air inlet temperature to the collector (Eq. (34), right side) which generally is a known parameter in each application.

The instantaneous collector efficiency is calculated by any of the two following expressions:

$$\eta_c = \frac{Q_u}{A_c G_p} = \frac{\dot{m} c_p (T_o - T_i)}{A_c G_p} = F_R\left(\frac{S}{G_p}\right) - F_R U_L \frac{(T_i - T_a)}{G_p} \tag{36}$$

Determining the instantaneous efficiency curve is of utmost importance to estimate the useful energy that the collector may produce according to the prevailing weather conditions at the site where it will be installed. In turn, it allows the estimation of the collection area necessary to satisfy a given demand for hot air. To determine its value it is necessary to know the total mass flow of the air passing through the collector.

This model is applicable to double parallel flow solar air collectors by natural or forced convection, with flat or V-corrugated absorber plate. In this paper, the model is validated by testing a double parallel flow solar collector by natural convection with a V-corrugated absorber plate, vertically installed.

3. Experimental evaluation of thermal performance of a solar air heater by natural convection

In order to validate the mathematical model, an experimental evaluation of the thermal performance of a double parallel flow solar air collector by natural convection, vertically mounted on the north facade (toward the Ecuador) of a building prototype, was carried out. This solar collector was designed and experimentally tested by the authors of this paper.

3.1. Description of the solar air heater and test methodology

The dimensions of the collector are: 2.22 m long, 0.94 m wide and 0.1 m thick. In the back it has two openings that connect the collector with the local to be heated through ducts that cross the wall. The bottom and sides of the collector box were thermally insulated with glass wool 5 cm thick. The transparent cover consists of two polycarbonate sheets with a sealed air chamber between them. The absorber plate is a V-corrugated galvanized sheet of 0.85 mm thick, 2.14 m long and 0.91 m wide, painted with black paint for high temperature. The corrugated angle is $\phi = 127°$ and the aperture area of the collector $A_c = 1.94$ m^2.

In Fig. 2, a diagram of the interior of the solar collector is shown. It is noted that the absorber plate has two upper and lower openings to allow the air to flow in contact with both sides of the plate in distributed way all over its surface. The sum of the areas of the two upper openings equals the cross area of the duct that communicates the collector with the building. The same is valid for the lower openings.

The solar radiation passing through the transparent cover is absorbed in the absorber plate, raising its temperature. The air in contact with the hot plate decreases its density and ascends by buoyancy, entering to the building through the upper duct. Simultaneously, the cold air located on the room floor is sucked toward the collector through the lower duct. Thus, a natural convective circulation between the collector and the building is established without there being any fan that forces this movement.

The solar collector was vertically installed on the north wall of a building prototype with 7.15 m^2 of floor area built at the National University of Salta in Salta City, Argentina (24° 43.7′ South Latitude, 65° 24.6′ West Longitude and 1200 m above sea level), as shown in Fig. 3. Its walls are made of hollow ceramic brick 15 cm thick. The roof is metallic, built with galvanized trapezoidal sheets and the floor is made of concrete 10 cm thick. Expanded polystyrene plates 5 cm thick conform a thermal insulated ceiling under the cover of galvanized sheets. The carpentries are made of pine wood and consist of a door toward east and a window of single glass toward west. All these materials are commonly used in the construction of social housing, although the ceramic bricks are also part of the multi-story buildings and of many houses of the richest social sectors of our country. That is, in terms of the characteristics of its envelope, the prototype monitored represents to a vast sector of the typical buildings of Argentina. The azimuth of north facade is 170° (10° to East from the North).

By means of K-type thermocouples connected to a data logger with 8 analogue channels were monitored, at intervals of 1 min, the temperatures of:

1) The air at the inlet and outlet solar collector,
2) The inner face of inner polycarbonate sheet,
3) The absorber plate at its geometric centre,
3) The two air drafts to the average distance between input and output and
4) The indoor air of the building prototype.

The external temperature and solar irradiation on the collector's vertical plane were monitored, also at intervals of 1 min, using an autonomous weather station whose pyranometer is photovoltaic. The air velocity at the collector inlet, necessary to estimate the circulating mass flow, was manually sensed by means of a hot wire anemometer.

The thermal behaviour of the solar collector was monitored during the winter of 2015. In this paper, the results for the period from July 27 to 31 are presented. This experimental evaluation allowed analyzing the dynamic behaviour of the solar air heater under real operating conditions (closed circuit collector-building).

3.2. Meteorological variables and temperatures measured in the solar collector

In Fig. 4, the values measured every 10 min of the ambient temperature, T_a, and of the global solar irradiance on the vertical plane of the collector, G_p, are represented.

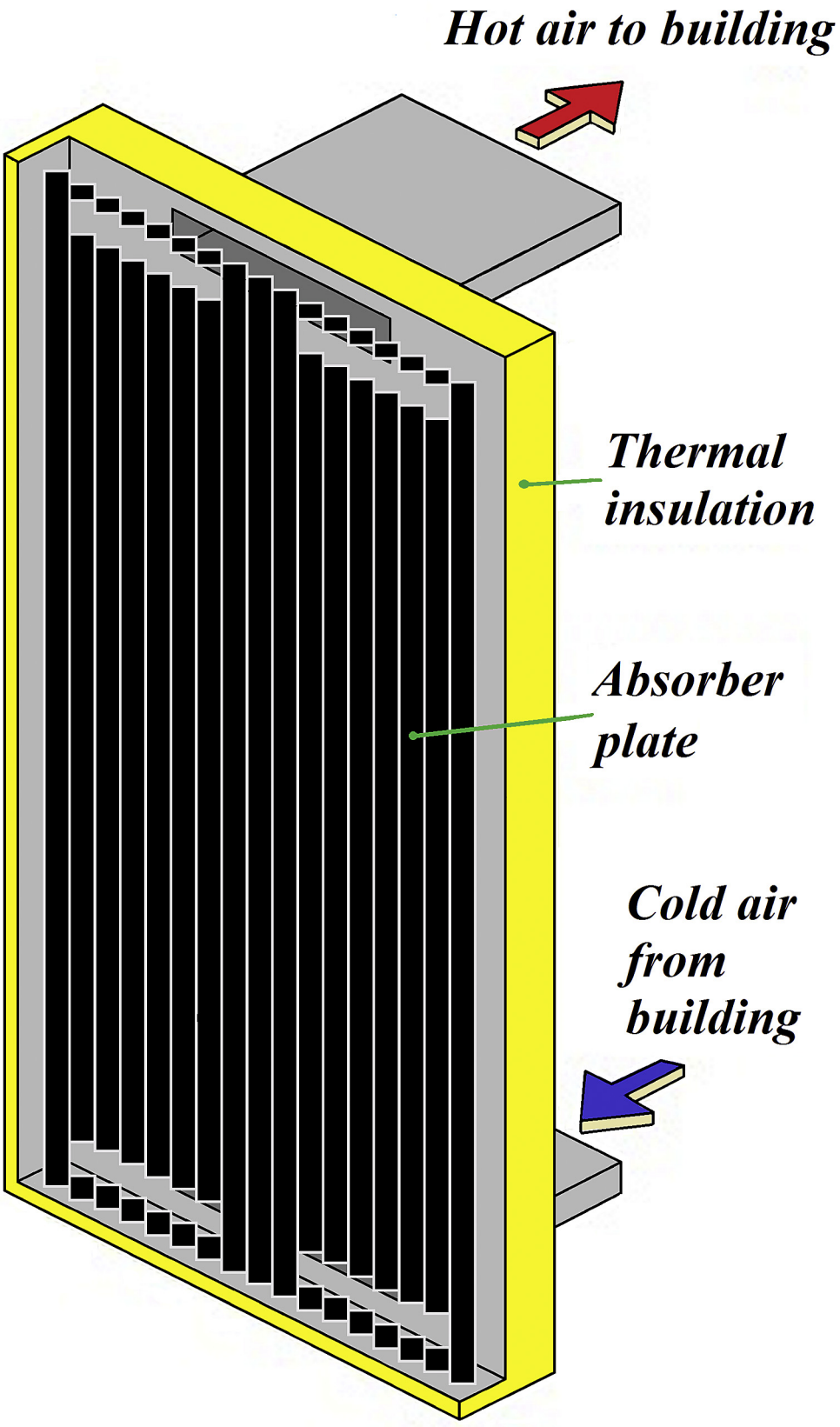

Fig. 2. Schematic section of solar collector.

Fig. 3. Solar air collector installed for testing.

As shown in the figure, the first days were sunny, registering typical values of ambient temperatures for this time of the year: minimum in the order of 0 °C and maximum between 16 and 18 °C. The statistical mean values recorded in previous decades in Salta City determined for July an average monthly value of 9.9 °C and an average monthly maximum of 20 °C. During the first three days plotted, solar irradiance on the vertical plane of the collector, G_p, reached maximum values of 710 W/m^2 at noon. The solar irradiance estimated by model of Souster et al. [39] for "clear day" gives a maximum of 790 W/m^2 on a vertical plane with azimuth of 170°, indicating scarce presence of suspended particulate matter in the local atmosphere.

Fig. 5 shows the air temperature values measured every 10 min at the collector inlet (T_i), at the output (T_o), of the air passing between the absorber plate and the transparent cover (T_{f1}), of the air passing between the absorber plate and bottom of the collector (T_{f2}) and the indoor air temperature of the space to be heated (T_l).

The figure shows that, during sunny days, the temperature of the air outlet overcomes 60 °C at noon, reaching a maximum value of 61 °C on July 28 when the solar irradiance on the plane of the collector was 710 W/m^2. The mechanism of the airflow by natural convection starts with very low values of solar irradiance since the outlet temperature begins its quick rise around 9:00 a.m., a time when the solar irradiance outside the collector is less than 100 W/m^2 as seen in Fig. 4. As the hot air comes out through the upper duct, it mobilizes room air and begins to rise its temperature and the temperature of inlet air to the collector.

Due to the heat supplied by the solar collector, the temperature of the room steadily rises during sunshine hours, reaching maximum values between 21 and 26 °C during the measurement period. In Fig. 5, the existence of thermal stratification in indoor air is observed since the temperature of the room (sensed at a height of 1.6 m) is always higher than that of the collector inlet (measured at a height of 0.3 m). During the night the temperature of the room descend to 15 °C which, although it is outside the range of thermal comfort in buildings (20–26 °C), is acceptable considering that the walls of the building does not have thermal insulation. With the useful heat provided by the collector on sunny days, the average daily temperature of the room (20 °C) exceeded in 12 °C the average outside temperature.

In Fig. 5 it is observed that, as predicted by the mathematical model, the temperature of the fluid passing in contact with the transparent cover, T_{f1}, is lower than that of the air passing in contact with the bottom of the collector, T_{f2}.

Fig. 6 shows the temperature values measured every 10 min at

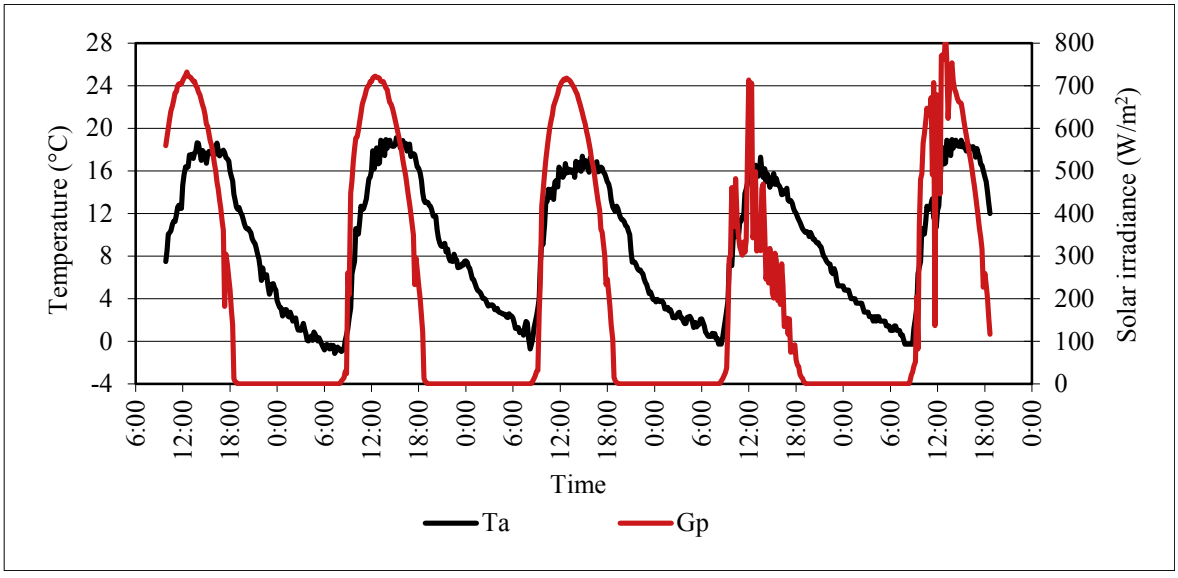

Fig. 4. Meteorological variables measured during the period from July 27 to 31.

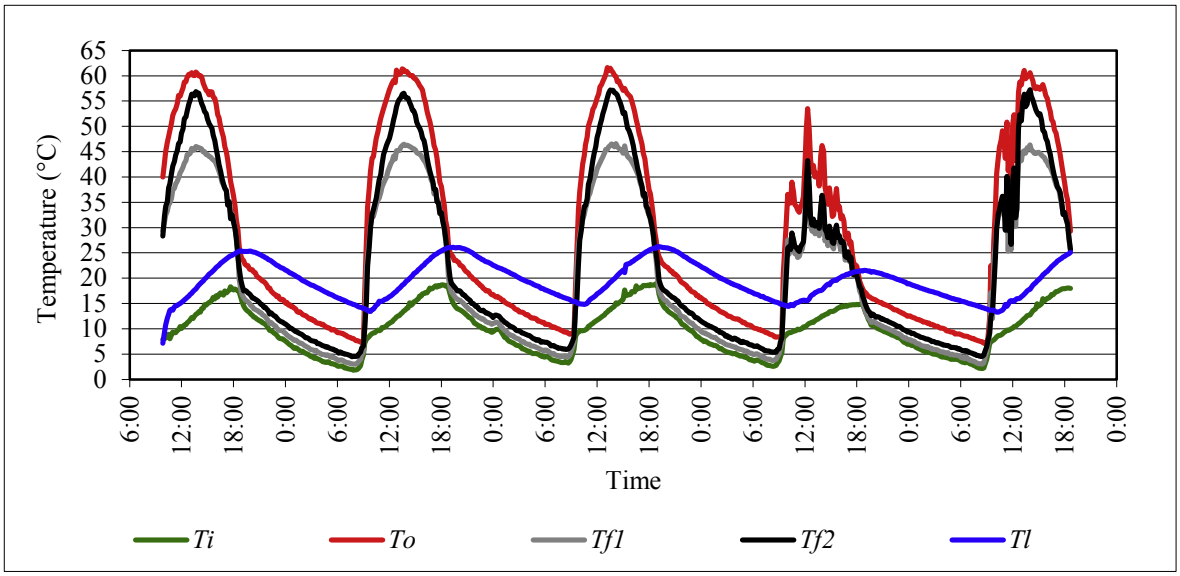

Fig. 5. Time evolution of input temperature (T_i), output (T_o), fluid 1 (T_{f1}), fluid 2 (T_{f2}) and inside of building (T_l).

the bottom of the solar collector (T_b), of the absorber plate (T_p) and of inner polycarbonate sheet (T_c) in their geometric centres. Due to the low speed values that characterize the movement of the air by natural convection, the temperature of the absorber plate increased to 68 °C in sunny days. As it is known, high values of the absorber plate temperature lead to low values of thermal efficiency.

During sunshine hours, the temperature of the cover is higher than that of the bottom of the collector mainly due to the radiative heat exchange with the hot absorber plate while, at night, the temperature of the cover is lower than that of the bottom due to radiative and convective heat exchange with the outside environment which is at very low temperature. Radiative exchange between the absorber plate and the cover is greater than between the absorber plate and the bottom of the collector because the absorber plate is painted black just by the side receiving solar radiation. The infrared emittances of paint used and of polycarbonate of transparent cover are greater than 0.94, while the back of the absorber plate and the bottom of the collector have infrared emittances of 0.2 corresponding to galvanized iron unpainted.

3.3. Air mass flow at solar collector inlet

In Fig. 7, the air velocity values measured at the inlet duct to the collector during the four sunny days are presented depending on the time of the day. These days were selected because in them the highest solar irradiance values were recorded. The curve is not symmetric about noon because the azimuth of the collector is slightly turned to the east as a result of the orientation of the building on which it was installed.

From 09:00 to 10:00 in the morning, the air velocity at collector inlet quickly increases from 0 to 0.75 m/s and in the next hour slowly reaches its maximum daily value. Between 11:00 and 13:00 h the air velocity remains quasi constant at a value close to 0.8 m/s. Since then the velocity begins to decrease slowly at first

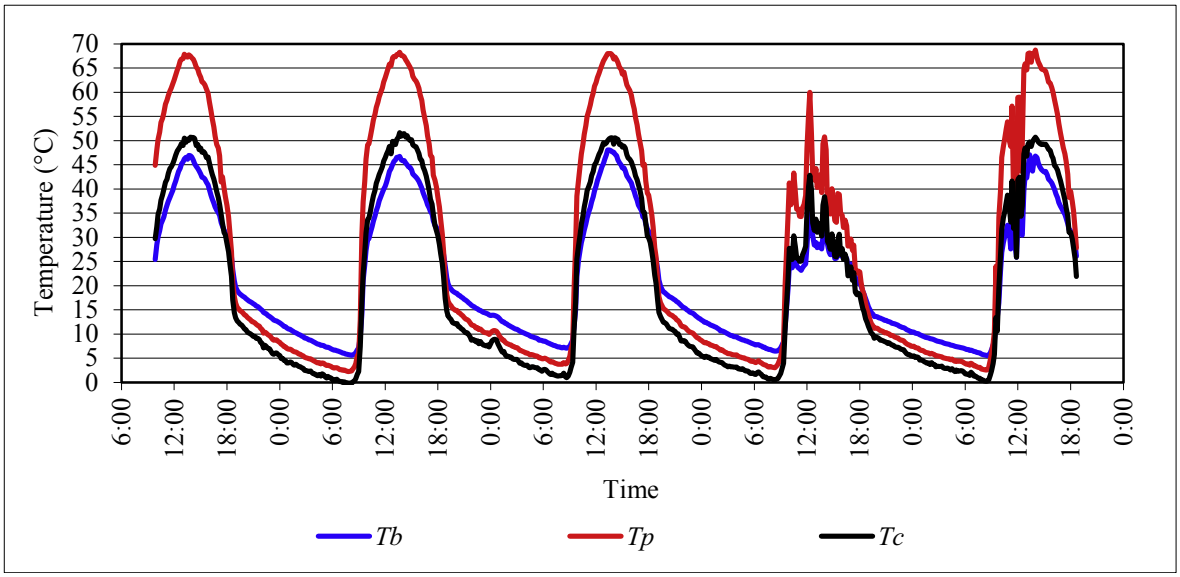

Fig. 6. Temperatures at the bottom of the collector (Tb), of the absorber plate (Tp) and the transparent cover (Tc), measured between July 27 and 31.

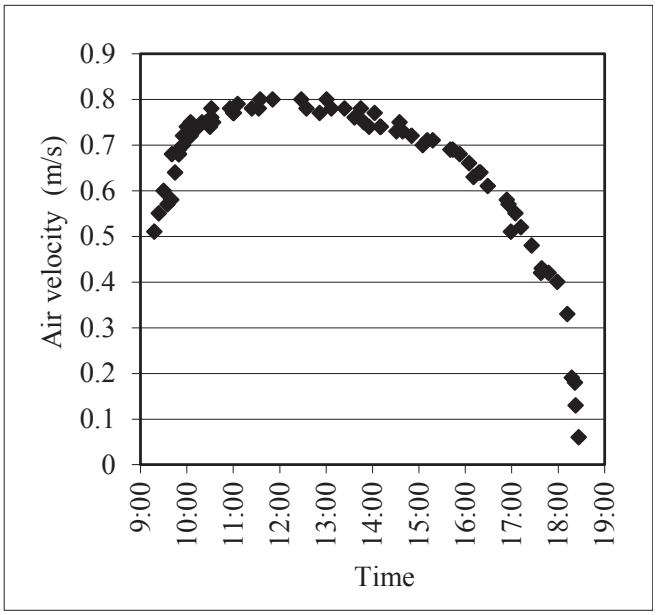

Fig. 7. Air velocity values measured at the inlet duct of the collector.

(until 16:00) and quickly thereafter until to be annulled approximately at 18:30. Therefore, between 10:00 and 15:30 h, the air velocity at collector inlet reached values between 0.7 and 0.8 m/s (87–100% of its maximum value for the weather conditions recorded during monitoring).

The air velocity at the collector inlet was measured manually at variable intervals between 5 and 60 min, from sunrise to sunset during the 5 days of monitoring. To estimate the instant useful energy gain to be used in the numerator of Eq. (36) it is necessary to obtain a continuous function that correlates the air velocity at the collector inlet with some variables measured during the test.

Locally, at any point x along a vertical hot plate with uniform temperature T_p, the solution to the Navier-Stockes equation for laminar airflow by natural convection, using the Boussinesq approximation, states that the local velocity profile of the air in contact with the hot plate, $u(x)$, is proportional to the local Grashof number, Gr_x, through an expression of the type [40]

$$u(x) \propto \frac{2\nu}{x} Gr_x^{1/2} = \frac{2\nu}{x}\left[\frac{g\beta(T_p - T_\infty)x^3}{\nu^2}\right]^{1/2} \tag{37}$$

where T_∞ is the air temperature abroad of thermal boundary layer. Rearranging the terms in Eq. (37), the following expression is obtained:

$$u(x) \propto \left[g\beta(T_p - T_\infty)x\right]^{1/2} \tag{38}$$

This approximation indicates that the air velocity inside the collector increases with increasing temperature of hot plate. Also indicates that the air velocity in the flow direction increases as $x \rightarrow L$. If L is large enough, at some point along the plate, the transition of laminar to turbulent regime occurs and Eq. (38) is no longer valid.

While Eq. (38) is useful to find out what parameters influence the determination of the air velocity inside the collector, its application to determine the average velocity at the input of the collector has two drawbacks. First, the temperature of the absorber plate in the flow direction is not uniform and its spatial distribution is unknown in the range $0 \leq x \leq L$. On the other hand, air temperature, T_∞, varies between the inlet and outlet of the solar collector and, usually, only its values at these two positions (T_i and T_o) are known. It is therefore more convenient to work with a global character equation that depends on these two known temperatures.

A solution of this type was presented by Duffie & Beckman [41] for a Trombe wall with small upper and lower openings for thermosiphon circulation. Solving the Bernoulli equation along a current line between the room to be heated and the flow channel of Trombe wall, the following expression for the average air velocity within the channel is obtained:

$$\overline{V} = \left[\frac{2gL}{C_1\left(A_g/A_i\right)^2 + C_2}\left(\frac{T_m - T_l}{T_m}\right)\right]^{1/2} \tag{39}$$

where L the height between the top and bottom openings, T_m the average air temperature between these openings, T_l the temperature of the room and C_1 and C_2 two dimensionless empiric constants related to the pressure drop in the Trombe channel (with cross area A_g) and openings (with cross area A_i). Whereas the denominator of the left fraction of Eq. (39) is a constant for each Trombe wall we can write the following proportionality relationship:

$$\overline{V} \propto \left[g\beta(T_m - T_l)L\right]^{1/2} \tag{40}$$

being $\beta = 1/T_m$ the volumetric thermal expansion coefficient of the air under the ideal gas approximation, with T_m and T_l in K. This relationship is morphologically similar to (38) but it has the advantage of including parameters and global variables measured during monitoring of the solar collector. The relationship (40) is also valid for the air velocity in the inlet duct of the collector because the continuity equation (mass conservation) states that:

$$v_i = \frac{\rho_m A_g}{\rho_l A_i}\overline{V} \tag{41}$$

where ρ_m is the air density at T_m temperature and ρ_l the air density at T_l temperature. Plotting the squared v_i values of Fig. 7 as a function of the variable $x = gL(T_m - T_l)/T_m$, the linear correlation of Fig. 8 is obtained.

The figure shows that the plotted data correlate linearly with an R^2 coefficient of 0.943. Most dispersion occurs for air velocities higher than 0.65 m/s ($v_i^2 \sim 0.42$ m^2/s^2). Then, the air velocity by natural convection at the collector inlet can be estimated by the following equation:

$$v_i = \left[0.0843 + 0.4332.g.L.\left(\frac{T_m - T_l}{T_m}\right)\right]^{1/2} \tag{42}$$

This correlation is a valuable tool to develop software of calculation and simulation of the performance of this collector type because it allows estimating the air mass flow circulating by natural convection.

In Fig. 9, the air velocity values measured at the collector inlet versus the estimated values with Eq. (42) are compared. An excellent agreement for velocities lower than 0.65 m/s, with a mean square error *RMSE* of 0.03 m/s and a mean square percentage error *RMSE%* of 4.5% throughout the velocity range analyzed, is observed.

As previously stated, in a solar collector of natural convection the air motion is due to the decrease of its density as it is heated in contact with the absorber plate. The air density dependence on the temperature is given by Ref. [42]:

$$\rho(T) = \rho_o[1 - \beta(T - T_o)] \quad \left(\mathrm{Kg}/\mathrm{m}^3\right) \tag{43}$$

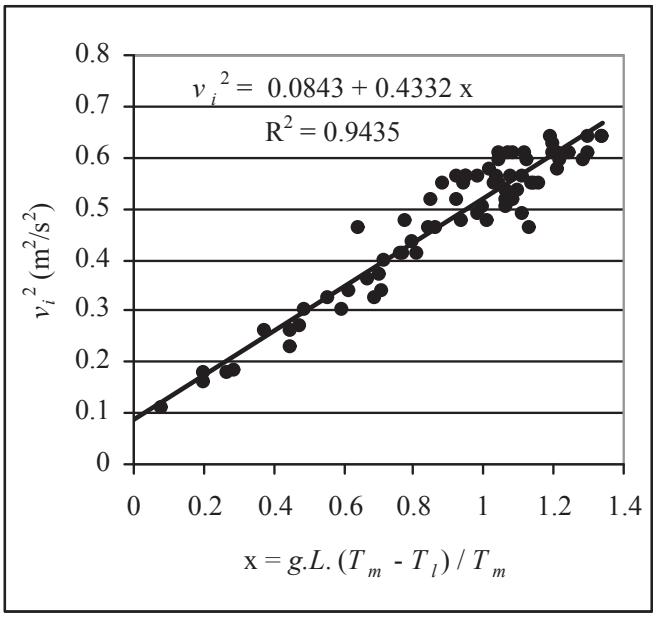

Fig. 8. Linear correlation of square air velocity at the collector inlet with T_m and T_l temperatures.

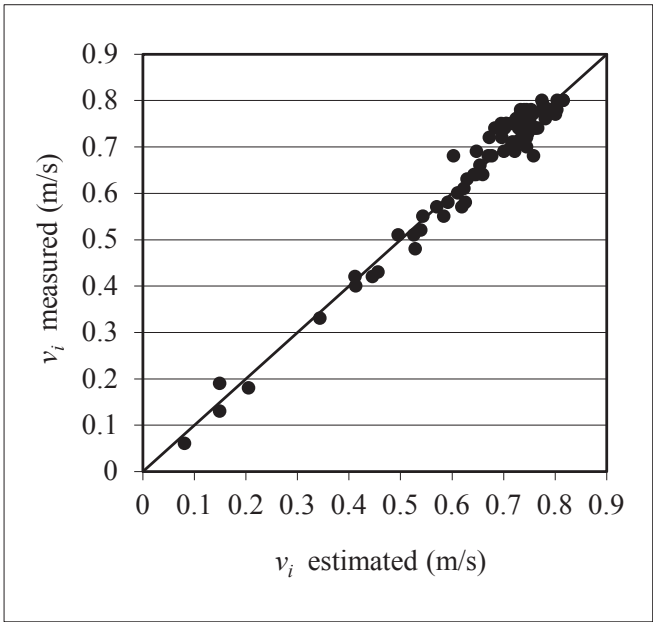

Fig. 9. Comparison between air velocity values measured and estimated with Eq. (42).

where T and T_o are absolute temperatures in K, ρ_o is the air density at T_o and $\beta = 1/T$ under ideal gas approximation. Replacing the value of β in Eq. (43) we obtain:

$$\rho(T) = \frac{\rho_o T_o}{T} = \frac{Const.}{T} \tag{44}$$

Therefore, the air density dependence on the temperature is not linear but hyperbolic.

The ideal gas approximation is valid for air at atmospheric pressure within the temperature range recorded during the operation of a solar air collector. Atmospheric pressure depends on the altitude above sea level of the place (H) and its value can be estimated by means of:

$$P(H) = 101,325(288.15/T_H)^{-5.255877}\ \text{(Pa)} \tag{45}$$

Where

$$T_H = 288.15 - 0.0065\,H \tag{46}$$

with T in K and H in meters, expressions valid for U.S. Standard Atmosphere, 1976 [42].

Therefore, Eq. (44) must be corrected by pressure multiplying it by a factor $P(H)/101{,}325$. Finally, the air mass flow, $\dot{m}$, is obtained by multiplying its density by the circulating flow rate and this, by multiplying the average fluid velocity, v_m, by the flow area, A_f, resulting:

$$\dot{m}(T,v) = \rho(T,H)v_m A_f = \frac{P(H)}{P_o}\frac{\rho_o T_o}{T} v\, A_f (Kg/s) \tag{47}$$

being $\rho_o = 1.2929$ kg/m^3 at $T_o = 273.13$ K and $P_o = 101{,}325$ Pa [40]. With this equation can be determined, hour by hour, the mass flows of the air in each channel of the solar collector through Eqs. (30) and (31) when the air velocity is known in the inlet duct, Eq. (42). The outlet temperature is calculated using Eq. (33), the useful energy gain with Eqs. (34) and (35) and the instantaneous collection efficiency with Eq. (36).

Replacing the value $H = 1200$ m in Eq. (46), the atmospheric pressure in Salta City is $P(H) = 87{,}715$ Pa. Therefore, in Eq. (47) the factor $P(H)/P_o = 0.86$. Because the air velocity was measured at the inlet duct to the collector whose area is $A_i = 0.0188$ m^2, the circulating mass flow at the inlet temperature (in K) is:

$$\dot{m}(T_i,v) = \rho(T_i,H)v_i A_i = 0,86\frac{\rho_o T_o}{T_i}v_i 0.0188 = 5.7094\frac{v_i}{T_i} \quad (Kg/s) \tag{48}$$

In Fig. 10, the time evolution of the air mass flow, estimated with Eq. (48), is shown. This curve has the similar behaviour than the solar irradiance G_p, with low values during the first and last hours of day and a maximum value at solar noon. During the sunny days, the average value between 10:00 and 15:30 h (58% of the total insolation period) is 0.015 kg/s.

3.4. Instantaneous thermal efficiency and useful energy produced

For determining the thermal efficiency curve, the values of solar irradiance, air temperatures of input and output, inner temperature of the building and outdoor temperature, recorded every 10 min during the 3 completely sunny days were selected and Eq. (48) was used to estimate the air mass flow at the collector inlet.

Using the first expression of Eq. (34), the thermal efficiency values were calculated and plotted as a function of the variable $(T_i - T_a)/G_p$. Finally, a least squares fit was applied to the data in order to obtain the linear regression function included in Fig. 11.

According to the results of Fig. 11, the instantaneous thermal efficiency curve of this solar air collector by natural convection is:

$$\eta_c = 0,45 - 10,08\frac{(T_i - T_a)}{G_p} \tag{49}$$

In Fig. 12, the measured values of the useful energy produced by the collector and the values estimated with instantaneous efficiency curve for the 5 days of monitoring are compared. The corresponding equations are [41]:

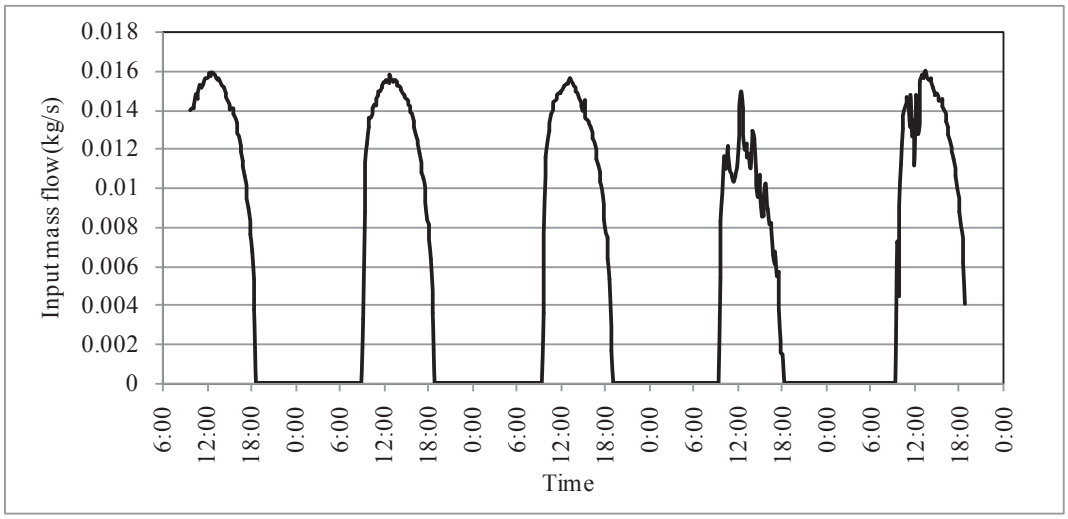

Fig. 10. Time evolution of de air mass flow at the inlet duct of the collector.

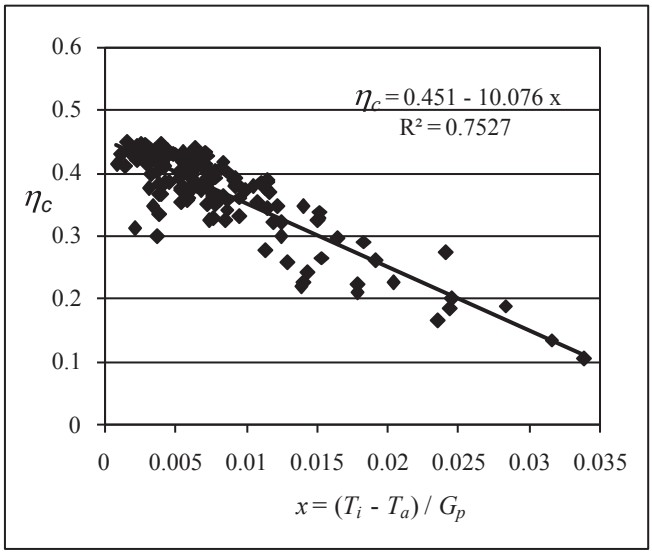

Fig. 11. Instantaneous thermal efficiency curve of the solar air collector of 1.94 m^2 net area.

$$\begin{aligned} Q_u\text{measured} &= \dot{m}\, c_p(T_o - T_i) \\ Q_u\text{estimated} &= \eta_c A_c G_p \end{aligned} \tag{50}$$

The dependence of the air specific heat on the temperature was included by means of a second-degree polynomial obtained by correlation of table values [40]:

$$c_p(T) = 1005.5 + 0.0282\,T + 0.0003\,T^2 \ \ (\text{J/kg°C}) \ \text{ with } T \text{ in } ^\circ\text{C} \tag{51}$$

The figure shows a very good agreement between measured and estimated values during sunny days and a relatively good fit for partly cloudy and cloudy days. To analyze the quality of fit between measured and simulated values, the root mean square error, *RMSE*, and the root mean square error percentage, *RMSE%* are defined as

$$RMSE = \sqrt{\frac{\sum_i (x_{m,i} - x_{s,i})^2}{N}} \tag{52}$$

$$RMSE\% = \sqrt{\frac{\sum_i \left[\frac{(x_{m,i} - x_{s,i})}{x_{m,i}}\right]^2}{N}} \text{x } 100 \tag{53}$$

where x_m and x_s respectively correspond to the measured and simulated values. These errors quantify the average deviation of the simulated values respect to the measured ones. Considering only the three sunny days, the *RMSE* is 50 W and the *RMSE%* 9.8%. That is, the instantaneous efficiency curve empirically obtained for the collector tested allows to estimate its useful energy gain with an average error of 10% for weather conditions of sunny days.

By integrating the measured values of useful energy produced by the collector and of global solar irradiance on the collector plane from sunrise to sunset, the daily values shown in Table 1 were obtained. The daily solar collection efficiency is defined as the ratio between the daily values of Q_u and global solar irradiation on the collector plane H_p.

The average daily thermal efficiency during the 3 sunny days was 48.7%, producing an average useful energy of 17.45 MJ by day. These efficiency values are in agreement with those reported in Ref. [24] and indicates that this solar air heater by natural convection has a very good thermal-energetic performance because it provides a large amount of thermal energy in a completely passive way, without requiring intervention or operation of building users. As shown in Fig. 5, a single module of this collector is sufficient to achieve thermal comfort conditions in a room of 18 m^3 volume (as studied in this paper) for meteorological winter conditions registered in Salta city (continental subtropical climate at 1200 m above sea level).

3.5. Heat transfer coefficients

According to Eq. (3), the amount of heat transferred by convection from the absorber plate to the air flowing through the collector is:

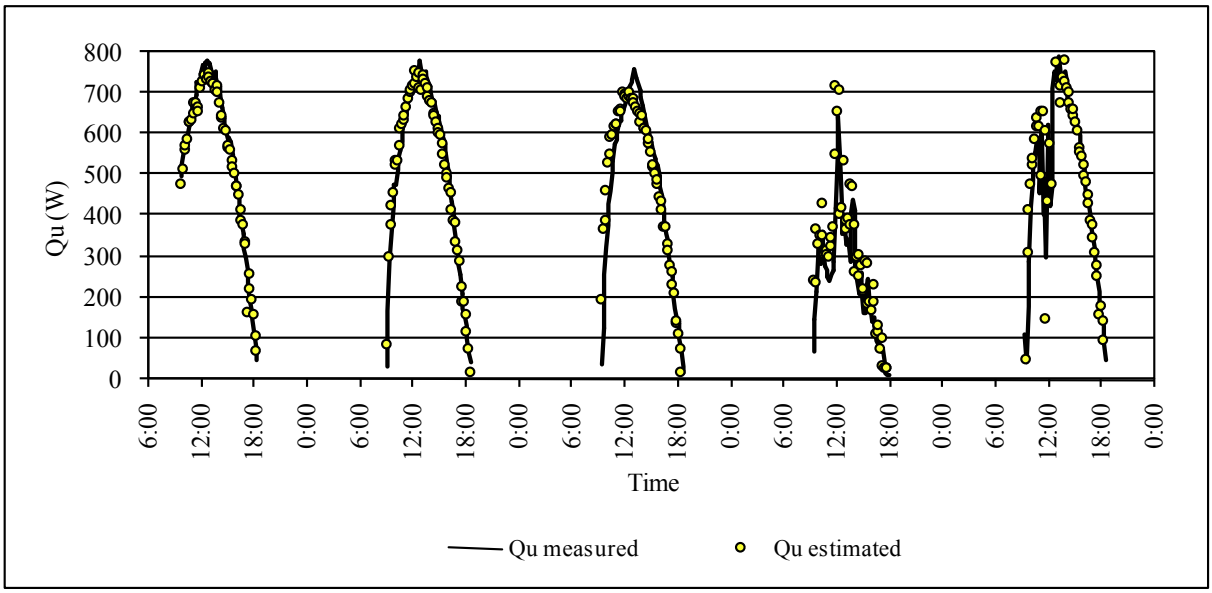

Fig. 12. Comparison between measured values of useful energy gain and simulated values using the thermal efficiency curve.

Table 1
Daily values of Q_u, of global solar radiation on the collector plane and of thermal efficiency measured from 27 to 31 July 2015.

Date	Q_u (MJ/day)	H_p (MJ/day)	η daily
27/07/09	17.44	34.47	0.50
28/07/09	17.83	37.11	0.48
29/07/09	17.07	35.53	0.48
30/07/09	7.79	18.95	0.41
31/07/09	16.22	35.21	0.46

$$h_2\left(T_p - T_{f1}\right) + h_3\left(T_p - T_{f2}\right) = S - h_{r1}\left(T_p - T_{c1}\right) - h_{r2}\left(T_p - T_b\right) \tag{54}$$

The terms on the right side of equation may be calculated from the data measured by means of [42]:

$$S = \left(\tau_b\alpha_p\right)G_bR_b + \left(\tau_d\alpha_p\right)G_{ds}\left(\frac{1+\cos\beta_c}{2}\right) + \left(\tau_g\alpha_p\right)G_h\rho_g\left(\frac{1-\cos\beta_c}{2}\right) \quad \left(\mathrm{W/m^2}\right) \tag{55}$$

$$h_{r1} = \frac{\sigma\left(T_p^2 + T_{c1}^2\right)\left(T_p + T_{c1}\right)}{\frac{\left(1-\varepsilon_{c1}\right)}{\varepsilon_{c1}} + \frac{1}{F_{12}} + \frac{\left(1-\varepsilon_p\right)A_{c1}}{\varepsilon_pA_p}} \quad \left(\mathrm{W/m^{2\circ}C}\right) \tag{56}$$

$$h_{r2} = \frac{\sigma\left(T_p^2 + T_b^2\right)\left(T_p + T_b\right)}{\frac{\left(1-\varepsilon_b\right)}{\varepsilon_b} + \frac{1}{F_{12}} + \frac{\left(1-\varepsilon_p\right)A_b}{\varepsilon_pA_p}} \quad \left(\mathrm{W/m^{2\circ}C}\right) \tag{57}$$

The two convective flows on the left side of Eq. (54) cannot be estimated from the measured data because h_2 and h_3 are unknown. However, it can be assumed that the heat is convectively transferred between the absorber plate and a fluid that is at the average temperature given by Eq. (15), resulting:

$$Q_c = h_{eff}\left(T_p - \left\langle T_f\right\rangle\right) \quad \left(\mathrm{W/m^2}\right) \tag{58}$$

where the effective heat transfer coefficient may be calculated as

$$h_{eff} = \frac{Q_c}{\left(T_p - \left\langle T_f\right\rangle\right)} = \frac{S + h_{r1}\left(T_{c1} - T_p\right) + h_{r2}\left(T_b - T_p\right)}{\left(T_p - \left\langle T_f\right\rangle\right)} \quad \left(\mathrm{W/m^2.^\circ C}\right) \tag{59}$$

by replacing the measured temperature data and the estimated values of S.

In natural convection processes, the convection heat transfer coefficient is usually estimated by correlating the dimensionless numbers Nu and Ra by means of an expression of the type:

$$Nu = C\ Ra^n \tag{60}$$

where C and n are constants to be determined from experimental data. The Nusselt number is defined as [40]:

$$Nu = \frac{h\,D_h}{k} \tag{61}$$

where h is the convective coefficient searched, k the thermal conductivity of air and D_h the hydraulic diameter of the flow channel. The Rayleigh number is given by Ref. [40]:

$$Ra = \frac{g\beta\left(T_p - T_\infty\right)D_h^3}{\nu\alpha} \tag{62}$$

Calculating the Nu number with the convective coefficient h_{eff} and Ra number with measured temperature values during the three sunny days of the monitoring period, the linear correlation of Fig. 13 (double logarithmic graph) was obtained.

The constants C and n respectively are 4.2948 ($e^{1.4574}$) and 0.2051 and the correlation (60) for natural convection is:

$$Nu = 4.2948\ Ra^{0.2051} \quad \text{for } 2.5 \text{ x } 10^5 < Ra < 1.3 \text{ x } 10^6 \tag{63}$$

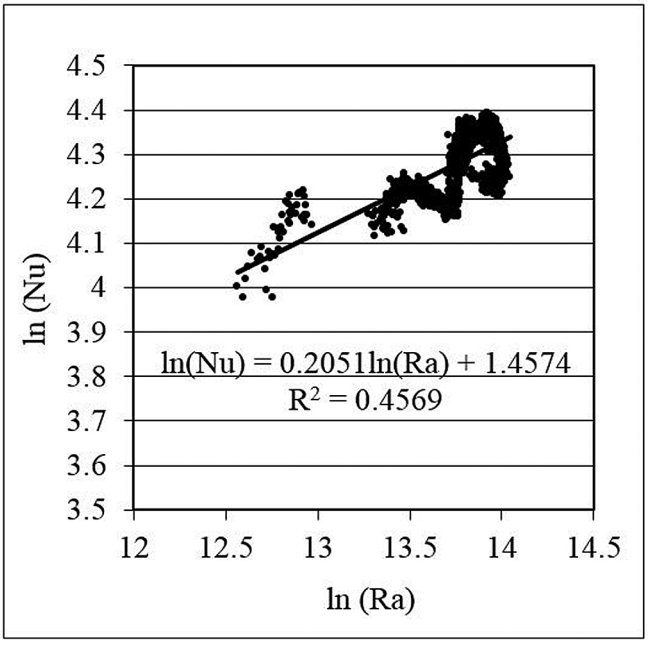

Fig. 13. Linear correlation of ln(*Nu*) versus ln(Ra).

The effective heat transfer coefficient is obtained from Eq. (61) as:

$$h_{eff} = \frac{Nu\ k}{D_h} \quad \left(\mathrm{W/m^2.^\circ C}\right) \tag{64}$$

The hydraulic diameter is calculated based on the transversal dimensions of the total flow channel of the collector [40]:

$$D_h = \frac{4 \times \text{Flow area}}{\text{Wetted perimeter}} = \frac{2w\,b}{(w+b)} \quad (\mathrm{m}) \tag{65}$$

Introducing Eqs. (15), (30) and (31) in (58) and rearranging the terms, the following expression is obtained:

$$h_{eff}\left(T_p - \left\langle T_f \right\rangle\right) = \left(\frac{\dot{m}_1}{\dot{m}} h_{eff}\right)\left(T_p - T_{f1}\right) + \left(\frac{\dot{m}_2}{\dot{m}} h_{eff}\right)\left(T_p - T_{f2}\right) \tag{66}$$

By comparing this result with the left side of Eq. (54), the following expressions for the two convective coefficients in contact with the absorber plate are obtained:

$$h_2 = \frac{\dot{m}_1}{\dot{m}} h_{eff}\left(T_p, T_{f1}\right) \text{ and } h_4 = \frac{\dot{m}_2}{\dot{m}} h_{eff}\left(T_b, T_{f2}\right) \tag{67}$$

where h_{eff} (T_p, T_f) is obtained from Eqs. (61)–(63) using as fluid temperature T_{f1} for h_2 and T_{f2} for h_3 in the *Ra* numbers calculation. With these expressions the coefficients h_1 and h_4 are also calculated as:

$$h_1 = \frac{\dot{m}_1}{\dot{m}} h_{eff}\left(T_{c1}, T_{f1}\right) \text{ and } h_4 = \frac{\dot{m}_2}{\dot{m}} h_{eff}\left(T_b, T_{f2}\right) \tag{68}$$

by replacing, in the respective *Ra* numbers, the absorber plate temperature T_p by T_{c1} for h_1 and by T_b for h_4.

In Table 2, the values in $\mathrm{W/m^{2\circ}C}$ of the 4 convective and 2 radiative coefficients, estimated with Eqs. (56), (57), (67) and (68) from temperature data measured in the double parallel flow solar air collector by natural convection, are presented.

It is observed in the table that the two convective coefficients for the air passing between the cover and the absorber plate are greater than those corresponding to the air passing through the other channel since $\dot{m}_1 > \dot{m}_2$. The radiative coefficient between the transparent cover and the absorber plate is much larger than the resultant between the absorber plate and the bottom surface of the collector because the black paint has an infrared emissivity of 0.95 (top face of the absorber) and the galvanized plate (underside face) has an emittance of 0.2.

Because the developed area of the V-corrugated plate is greater than the aperture area A_c by a factor $1/\sin(\phi/2)$, it must divide the numerical values of h_2 and h_3 by $\sin(\phi/2)$ in the expressions of F' and U_L, Eqs. (7) and (13) respectively.

4. Validation of the analytical model with the experimental test data

The values of input and output temperatures of the air, meteorological variables and air velocity measured at the collector inlet during the three sunny days were used to validate the mathematical model proposed by Hernández and Quiñonez [37]. The algebraic equations of the model (Eqs. (7)–(36)) and the empirical correlations to determine the heat transfer coefficients (Eq. (55)–(68)) were transformed into computational algorithms and coded in programming language Visual Basic. In this software, the geometrical data of the solar collector and the thermo-optical properties of the covers and the absorber plate are introduced as particular parameters according to the collector prototype evaluated. The time step for the simulation is 1 h.

In Fig. 14, the values of the air temperature measured at the collector outlet during the days 27, 28 and 29 July are compared with the simulated values through the mathematical model and, in Fig. 15, the values of useful energy produced by the collector are compared. In both figures, the experimental uncertainties associated with the calibration of sensors and the measurement processes were included. The temperature uncertainty is (±1 °C) and that of the useful energy (±47 W), obtained by errors propagation technique on Eq. (50), [43]. It is noted that the fit for both variables is significantly good, slightly overestimated by the model, with average differences lower than 1.5 °C in the air outlet temperature and 20 W in the useful energy produced as shown in Table 3.

The simulated curve corresponding to the air outlet temperature falls within the experimental error range in most of the points plotted in Fig. 14, especially during the second and third day, while the simulated curve for the useful energy always falls within the experimental error range as shown in Fig. 15. This confirms the excellent fitting achieved with the mathematical model evaluated in this work.

This is because the mathematical model complies with the first principle of thermodynamics and with the energy balance equation for fluids. The thermal properties of the air have been calculated considering their dependencies with pressure and temperature and were included the mass balance, the momentum balance (Eq. of Navier Stokes) and the Boussinesq approximation for the estimation of the air velocity by natural convection (Eq. (42)). Since the model fits reasonably well to the measured data we consider that the experimental results obtained in the collector test are realistic from the point of view of the physical principles involved.

Table 2
Estimated values of the heat transfer coefficients within the collector.

h_1	h_2	h_3	h_4	h_{r1}	h_{r2}
8.7	11.6	7.7	6.6	6.7	0.9

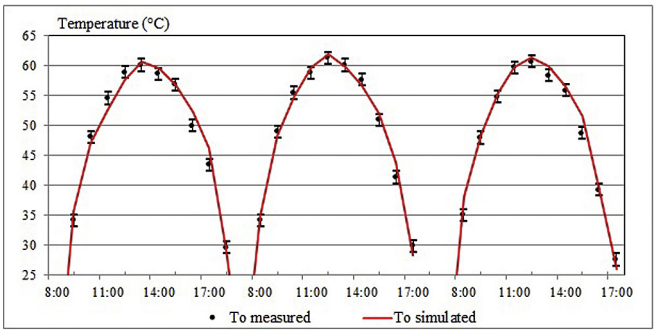

Fig. 14. Comparison between measured and simulated values of the air output temperature of the collector.

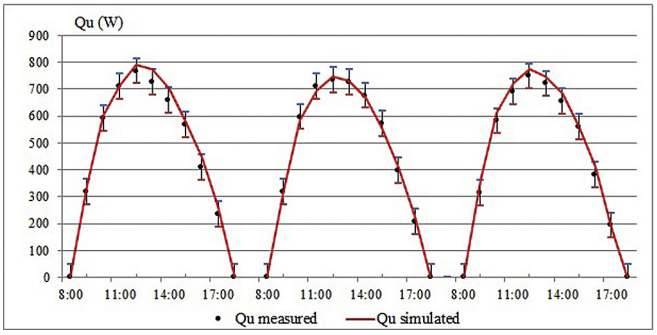

Fig. 15. Comparison between measured and simulated values of the useful energy produced.

Table 3
RMSE and RMSE% values for air output temperature and useful energy gain of the collector.

Variable	*RMSE*	*RMSE%*
Temperature, T_o	1.4 °C	3.7%
Useful energy, Q_u	20 W	5%

In Table 3, the values of *RMSE* and *RMSE%* during the 3 sunny days, corresponding to T_o and Q_u, are presented.

From the analysis of experimental uncertainties and percentage fit errors it is concluded that the numerical model is able to predict the thermal behaviour of this type of collectors with sufficient accuracy because it has an average error of only 3.7% in the fit of the air output temperature and of 5% for the useful energy produced, falling both curves within the experimental error.

5. Conclusions

In this paper, the thermal -energetic evaluation of a double parallel flow solar air collector by natural convection was presented. The work was developed at the National University of Salta, Argentina, during the winter of 2015. The instantaneous efficiency curve was determined experimentally and adjusted by linear regression with a correlation coefficient $R^2 = 0.75$. Daily values of thermal efficiency varied between 0.48 and 0.5 during sunny days and between 0.41 and 0.46 during the semi-cloudy days. These values are very satisfactory because the operation of the collector is by natural convection, without electric power consumption to move the fluid.

By means of linear regression, a novel correlation between the velocity of the air movement by natural convection and the temperature difference between the building and the collector's interior was obtained, with a correlation coefficient $R^2 = 0.94$. The air motion velocity depends on the square root of the distance between the input and output openings. Thus, the greater the length of the collector, the greater the mass flow established by natural convection and, consequently, the greater the instantaneous collection efficiency. An excellent agreement between measured and estimated values for velocities lower than 0.65 m/s, with a mean square error *RMSE* of 0.03 m/s and a mean square percentage error *RMSE%* of 4.5% was obtained. This correlation is a valuable tool to develop software of calculation and simulation of the performance of this collector type.

The installation of this collector on the north facade of the buildings allows to reduce the window area needed to achieve inner thermal comfort levels by direct solar gain, thus reducing the visual exposure of users and their belongings. Another of its advantages is that, by its steepness, collects energy mainly during the winter. In summer it is possible to shade it with an eave conveniently designed or with a light-coloured cover of to avoid the collection of diffuse solar radiation if the surrounding has a high albedo, since air movement by natural convection starts with values of solar irradiance as low as 100 W/m^2 on the plane of the collector.

Due to the proper characteristics of its functioning, it is recommended to use this collector type to heat spaces of diurnal use as classrooms, libraries or reading rooms, waiting rooms in hospitals, public offices, industrial workshops and living rooms, among others.

A new correlation $Nu = f(Ra)$ for natural convection was obtained based on an effective convective heat transfer coefficient h_{eff}, calculated with temperature values measured inside the collector and the absorbed solar irradiance, S. This correlation was used to estimate the four average convective coefficients inside the collector, h_1 to h_4. The two convective coefficients for the air passing between the cover and the absorber plate are greater than those corresponding to the air passing through the other channel since $\dot{m}_1 > \dot{m}_2$. If the absorber plate is V-corrugated, the convective coefficients h_2 and h_3 must be divided by $\sin(\phi/2)$ for the correct calculation of coefficients F' and U_L. The two radiative heat transfer coefficients h_{r1} and h_{r2} were estimated using correlations for parallel plates obtained from the literature.

Finally, the data of the air temperatures inside the collector and of meteorological variables obtained during the winter monitoring at the National University of Salta were used to validate an analytical model developed in a previous paper. The algebraic equations of the model and the empirical correlations to determine the heat transfer coefficients were transformed into computational algorithms and coded in programming language Visual Basic.

From the analysis of experimental uncertainties and percentage fit errors between measured and estimated values of the output temperature (3.7%) and the useful energy produced (5%) it is concluded that the numerical model is able to predict the thermal behaviour of this type of collectors with sufficient accuracy, validating in this way, the physical-mathematical model proposed.

Acknowledgment

The authors gratefully acknowledge the support provided by the Research Council of the National University of Salta (CIUNSa) and the National Scientific and Technical Research Council (CONICET) for financing this work.

References

[1] A. Sharma, C.R. Chen, N. Vu Lan, Solar-energy drying systems: a review,

Renew. Sustain. Energy Rev. 13 (2009) 1185–1210.
[2] A.A. El-Sebaii, S.M. Shalaby, Solar drying of agricultural products: a review, Renew. Sustain. Energy Rev. 16 (2012) 37–43.
[3] S. Vijaya Venkata Raman, S. Iniyan, Goic Ranko, A review of solar drying technologies, Renew. Sustain. Energy Rev. 16 (2012) 2652–2670.
[4] K.A. Joudi, A.A. Farhan, Greenhouse heating by solar air heaters on the roof, Renew. Energy 72 (2014) 406–414.
[5] A. Hernández, G. Lesino, L. Rodríguez, J. Linares, Design, modelling and computational assessment of passive and active solar collectors for thermal conditioning of the first bioclimatic hospital in Argentina, J. Build. Perform. Simul. 3 (3) (2010) 217–232.
[6] A. Hernández, M. Güizzo, J. Carracedo, E. Lisi, "SAMÍRI": vivienda bioclimática en Salta con techo-colector calentador de aire para su calefacción invernal, in: Revista Avances en Energías Renovables y Medio Ambiente (AVERMA), 2010, p. 14. Tema 5: 09–16.ISSN 0329-5184, http://www.cricyt.edu.ar/asades/averma.php (Last accessed 2 May 2017).
[7] L.H. Gunnewiek, E. Brundrett, K.G.T. Hollands, Flow distribution in unglazed transpired plate solar air heaters of large area, Sol. Energy 58 (4–6) (1996) 227–237.
[8] M.M. Sorour, Z.A. Mottaleb, Effects of design parameters on the performance of channel-type solar energy air heaters with corrugated plates, Appl. Energy 17 (3) (1984) 181–190.
[9] D. Alta, E. Bilgili, C. Ertekina, O. Yaldiza, Experimental investigation of three different solar air heaters: energy and exergy analyses, Appl. Energy 87 (10) (2010) 2953–2973.
[10] B.M. Ramani, A. Gupta, R. Kumar, Performance of a double pass solar air collector, Sol. Energy 84 (2010) 1929–1937.
[11] A.P. Omojaro, L.B.Y. Aldabbagh, Experimental performance of single and double pass solar air heater with fins and steel wire mesh as absorber, Appl. Energy 87 (12) (2010) 3759–3765.
[12] S. Bouadila, S. Kooli, M. Lazaar, S. Skouri, A. Farhat, Performance of a new solar air heater with packed-bed latent storage energy for nocturnal use, Appl. Energy 110 (2013) 267–275.
[13] K. Rajarajeswari, A. Sreekumar, Matrix solar air heaters – a review, Renew. Sustain. Energy Rev. 57 (2016) 704–712.
[14] A.A. Mohamad, High efficiency solar air heater, Sol. Energy 60 (2) (1997) 71–76.
[15] K. Pottler, C.M. Sippel, A. Beck, J. Fricke, Optimized finned absorber geometries for solar air heating collectors, Sol. Energy 67 (1–3) (1999) 35–52.
[16] K. Sopian, Supranto (Dr), W.R.W. Daud, M.Y. Othman, B. Yatim, Thermal performance of the double-pass solar collector with and without porous media, Renew. Energy 18 (1999) 557–564.
[17] N. Moummi, S. Youcef-Ali, A. Moummi, J.Y. Desmons, Energy analysis of a solar air collector with rows of fins, Renew. Energy 29 (2004) 2053–2064.
[18] R. Ben Slama, The air solar collectors: comparative study, introduction of baffles to favour the heat transfer, Sol. Energy 81 (2007) 139–149.
[19] C.D. Ho, H.M. Yeh, T.W. Cheng, T.C. Chen, R.C. Wang, The influences of recycle on performance of baffled double-pass flat-plate solar air heaters with internal fins attached, Appl. Energy 86 (9) (2009) 1470–1478.
[20] E. Kavak Akpinar, F. Koçyiğit, Energy and exergy analysis of a new flat-plate solar air heater having different obstacles on absorber plates, Appl. Energy 87 (11) (2010) 3438–3450.
[21] Ravi Kant Ravi, Rajeshwer Prasad Saini, A review on different techniques used for performance enhancement of double pass solar air heaters, Renew. Sustain. Energy Rev. 56 (2016) 941–952.
[22] Wenfeng Gao, Wenxian Lin, Enrong Lu, Numerical study on natural convection inside the channel between the flat plate cover and sine-wave absorber of a cross-corrugated solar air heater, Energy Convers. Manag. 41 (2000) 145–151.
[23] Yasin Varol, Hakan F. Oztop, A comparative numerical study on natural convection in inclined wavy and flat-plate solar collectors, Build. Environ. 43 (2008) 1535–1544.
[24] N. Hatami, M. Bahadorinejad, Experimental determination of natural convection heat transfer coefficient in a vertical flat-plate solar air heater, Sol. Energy 82 (2008) 903–910.
[25] Hussain H. Al-Kayiem, Tadahmun A. Yassen, On the natural convection heat transfer in a rectangular passage solar air heater, Sol. Energy 112 (2015) 310–318.
[26] A. Hernández, N. Salvo, C. Fernández, H. Suligoy, Diseño y evaluación térmica de un colector solar calentador de aire de placa perforada para calefacción de edificios, in: Avances en Energías Renovables y Medio Ambiente (AVERMA), 2008, p. 12. Tema 3: 133–140, http://www.cricyt.edu.ar/asades/averma.php (Last Accessed 02 May 2017).
[27] A.A. Hegazy, Performance of flat plate solar air heaters with optimum channel geometry for constant/variable flow operation, Energy Convers. Manag. 41 (2000) 401–417.
[28] H.D. Ammari, A mathematical model of thermal performance of a solar air heater with slats, Renew. Energy 28 (2003) 1597–1615.
[29] Siddhartha Varun, Thermal performance optimization of a flat plate solar air heater using genetic algorithm, Appl. Energy 87 (5) (2010) 1793–1799.
[30] G. Leone, M. Beccali, Use of finite element models for estimating thermal performance of façade-integrated solar thermal collectors, Appl. Energy 171 (2016) 392–404.
[31] Wenfeng Gao, Wenxian Lin, Tao Liu, Chaofeng Xia, Analytical and experimental studies on the thermal performance of cross-corrugated and flat-plate solar air heaters, Appl. Energy 84 (4) (2007) 425–444.
[32] A.A. El-Sebaii, S. Aboul-Enein, M.R.I. Ramadan, S.M. Shalaby, B.M. Moharram, Thermal performance investigation of double pass-finned plate solar air heater, Appl. Energy 88 (5) (2011) 1727–1739.
[33] P. Dhiman, N.S. Thakur, A. Kumar, S. Singh, An analytical model to predict the thermal performance of a novel parallel flow packed bed solar air heater, Appl. Energy 88 (6) (2011) 2157–2167.
[34] C.D. Ho, H. Chang, R.C. Wang, C.S. Lin, Performance improvement of a double-pass solar air heater with fins and baffles under recycling operation, Appl. Energy 100 (2012) 155–163.
[35] Ming Yang, Xudong Yang, Xing Li, Zhifeng Wang, Pengsu Wang, Design and optimization of a solar air heater with offset strip fin absorber plate, Appl. Energy 113 (2014) 1349–1362.
[36] S.M. González, S. Flores Larsen, A. Hernández, G. Lesino, Thermal evaluation and modelling of a double-pass solar collector for air heating, Energy Proced. 57 (2014) 2275–2284.
[37] A. Hernández, J. Quiñonez, Analytical models of thermal performance of solar air heaters of double-parallel flow and of double-pass counter flow, Renew. Energy 55 (2013) 380–391.
[38] J.E. Quiñonez, A.L. Hernández, Evaluación y simulación computacional de un modelo físico-matemático del colector solar calentador de aire de doble paso en contracorriente diseñado para la calefacción de edificios, in: Avances en Energías Renovables y Medio Ambiente (AVERMA), 2013, p. 17. Tema 8: 21–28, http://www.cricyt.edu.ar/asades/averma.php (Last Accessed 02 May 2017).
[39] C.G. Souster, G.G. Rodgers, J.K. Page, The Development of an Interactive Computer Program SUN3 for the Calculation of Solar Irradiances and Daily Irradiations Incident upon Surfaces of Any Slope and Orientation on Cloudless Days for Given Conditions of Sky Clarity and Atmospheric Water Content, Technical Report, Department of Building Science, Faculty of Architectural Studies, University of Sheffield, U.K., 1978.
[40] F. y Incropera, D. DeWitt, Fundamentals of Heat and Mass Transfer, third ed., John Wiley & Sons, New York, 1990.
[41] J. A. y Duffie, W.A. Beckman, Solar Engineering of Thermal Processes, third ed., John Wiley & Sons, New Jersey, 2006.
[42] D. Lide, Handbook of Chemistry and Physics, 71st ed., CRC Press, Boston, 1990.
[43] A.A. Clifford, Multivariate Error Analysis: a Handbook of Error Propagation and Calculation in Many-parameter Systems, Applied Science Publishers, London, 1973.